Title	Enhanced indirect ferromagnetic p-d exchange coupling of Mn in oxygen rich ZnO:Mn nanoparticles synthesized by wet chemical method
Author(s)	Usman Ilyas, R. S. Rawat, T. L. Tan, P. Lee, R. Chen, H. D. Sun, Li Fengji and Sam Zhang
Source	*Journal of Applied Physics, 111*(3): 033503. doi: 10.1063/1.3679129
Published by	American Institute of Physics

Enhanced indirect ferromagnetic p-d exchange coupling of Mn in oxygen rich ZnO:Mn nanoparticles synthesized by wet chemical method

Usman Ilyas, R. S. Rawat, T. L. Tan, P. Lee, R. Chen et al.

Citation: J. Appl. Phys. **111**, 033503 (2012); doi: 10.1063/1.3679129
View online: http://dx.doi.org/10.1063/1.3679129
View Table of Contents: http://jap.aip.org/resource/1/JAPIAU/v111/i3
Published by the American Institute of Physics.

Enhanced indirect ferromagnetic p-d exchange coupling of Mn in oxygen rich ZnO:Mn nanoparticles synthesized by wet chemical method

Usman Ilyas,[1,2] R. S. Rawat,[1,a)] T. L. Tan,[1] P. Lee,[1] R. Chen,[3] H. D. Sun,[3] Li Fengji,[4] and Sam Zhang[4]
[1]*NSSE, NIE, Nanyang Technological University, 1 Nanyang Walk, Singapore 637616, Singapore*
[2]*Department of Physics, University of Engineering & Technology, Lahore 54890, Pakistan*
[3]*Division of Physics and Applied Physics, School of Physical and Mathematical Sciences, Nanyang Technological University, Singapore 637371, Singapore*
[4]*School of Mechanical and Aerospace Engineering, Nanyang Technological University, 50 Nanyang Avenue, Singapore 639798, Singapore*

(Received 3 September 2011; accepted 23 December 2011; published online 3 February 2012)

This paper investigates the ferromagnetism in ZnO:Mn powders and presents our findings about the role played by the doping concentration and the structural defects towards the ferromagnetic signal. The narrow-size-distributed ZnO:Mn nanoparticles based powders with oxygen rich stoichiometery were synthesized by wet chemical method using zinc acetate dihydrate and manganese acetate tetrahydrate as precursors. A consistent increase in the lattice cell volume, estimated from x-ray diffraction spectra and the presence of Mn $2p_{3/2}$ peak at ~640.9 eV, in x-ray photoelectron spectroscopic spectra, confirmed a successful incorporation of manganese in its Mn^{2+} oxidation state in ZnO host matrix. Extended deep level emission spectra in Mn doped ZnO powders exhibited the signatures of oxygen interstitials and zinc vacancies except for the sample with 5 at. % Mn doping. The nanocrystalline powders with 2 and 5 at. % Mn doping concentration were ferromagnetic at room temperature while the 10 at. % Mn doped sample exhibited paramagnetic behavior. The maximum saturation magnetization of 0.05 emu/g in the nanocrystalline powder with 5 at. % Mn doping having minimum defects validated the ferromagnetic signal to be due to strong p-d hybridization of Mn ions.
 [doi:10.1063/1.3679129]

I. INTRODUCTION

Presently, magnetic devices utilize only the spin degree of freedom of the electrons to bring about the functionalities regarding data storage in hard disks and magnetic random access memories based on metallic multilayers. Conventional electronics utilizes only the charge degree of freedom of the carriers to process the data. The emerging field of spintronics represents the convergence of two fundamental properties of electron, charge and spin, to form the basis for a new class of device design.[1] The exploitation of electron spin in practical devices has already been established as spin valves are used as magnetic tunnel junctions in magnetic random access memory (MRAM), a platform that aims to replace current memory technologies. One of the ingenious ways to combine the spin and charge of electrons in a material, and achieve these effects, is by synthesizing a material with both semiconducting as well as magnetic properties. Being a ferromagnetic semiconductor with favorable experimental properties, dilute magnetic semiconductors (DMSs) will promisingly suit this need. DMS have recently attracted broad interest for their promised functionalities in spintronics as the charge and spin of electrons are accommodated into single material leading to interesting magnetic, magneto-optical, and magneto-electric properties.[1,2] Magnetic properties of II-VI-based DMS have attracted much attention[3] after Dietl's prediction about the room temperature ferromagnetism (RTFM) in Mn-doped ZnO.[4] There has been a considerable interest in the fabrication of transition metal doped ZnO as a promising material for the discovery of RTFM in implementing spintronic devices.[5] Numerous studies have, therefore, been carried out to grow ZnO:Mn semiconductors due to large spin moment exhibited by Mn and is extensively investigated as a candidate element for producing ferromagnetic ZnO essential for magneto electronics and spintronic applications.[6–8] Although several groups have reported the ferromagnetic behavior of ZnO:Mn semiconductors,[9–13] but some reports exhibited non ferromagnetic nature of polycrystalline ZnO:Mn thin films at room temperature.[14–16] Some researchers reported defect mediated ferromagnetism due to zinc and oxygen vacancies (V_o) coupled with Mn ions[17,18] while the others reported the origin of ferromagnetism due to impurity phases such as nanoclustering of oxides of Mn and spinel $ZnMn_2O_4$ (Ref. 19) formation. Due to the controversial results indicated in literature, the origin of ferromagnetism is still in debate. In addition, the lack of reproducibility of ferromagnetic signal in ZnO:Mn based DMS materials prepared with the same manganese content raises questions about the origin of the ferromagnetism in ZnO:Mn.

In view of recent controversies in RTFM in transition metal doped ZnO, the present paper aims to shed some light on the origin of ferromagnetism by investigating Mn doped nanocrystalline ZnO powders for their structural, compositional, optical, morphological, and magnetic properties. The investigation of ZnO:Mn based DMS to optimize the synthesis and growth parameters of Mn doped ZnO nanocrystalline

a)Author to whom correspondence should be addressed. Electronic mail: rajdeep.rawat@nie.edu.sg.

powders is useful for spintronic applications. We report the RTFM due to strong hybridization of Mn ions in ZnO nanocrystalline powders synthesized through wet chemical method. The powder obtained from wet chemical method offers homogeneous doping of Mn in ZnO host matrix as compared to the powder obtained by commonly used solid-state reaction method. The role of structural defects and dopant concentration in ferromagnetic signal is also investigated and discussed.

II. EXPERIMENTATION

Nanocrystalline Mn doped ZnO powders were synthesized through a wet chemical method. The Mn-doped ZnO powders were prepared for three different Mn doping concentrations of 2, 5, and 10 at. % hereinafter referred as CP-2%, CP-5%, and CP-10%, respectively. Zinc acetate dihydrate (90 mMol) and manganese acetate tetrahydrate (2.9 mMol) were mixed along with potassium hydroxide (280 mMol) in an environment of methanol (50 ml) for the preparation of CP-2% sample. The solution was continuously stirred using a magnetic stirrer for 3 h at 52 °C to get homogeneous mixing in solution. It was then cooled to room temperature and allowed to age for 24 h. The fine precipitates were removed by centrifugation and washed repeatedly with distilled water to remove un-reacted materials. The precipitates were dried for one day and sintered at a temperature of 550°C for 2 h to get rid of byproducts from the samples. Zinc acetate dihydrate (Aldrich), manganese acetate tetrahydrate (Aldrich), potassium hydroxide (Baker), and methanol (Aldrich), in above mentioned preparation procedure, were used as received. Nanocrystalline powders of CP-5% and CP-10% were also prepared by the same procedure using suitable quantities of acetates and solvents.

The crystalline phase of nanocrystalline powders was analyzed using a SIEMENS D5005 Cu K_α (1.504 Å) x- ray diffractometer (XRD). Near band edge (NBE) and deep level emission (DLE) energy transitions from photoluminescence (PL) spectra, measured using Hd-Cd (325 nm and 10 mW) laser, were used to study the variation in optical band gap and structural defects with dopant concentration. X-ray photoelectron spectroscopy (XPS) with Kratos axis-ultra spectrometer equipped with a focused monochromatic Al-K_α (1486.6 eV) x-ray beam (15 kV and 10 mA) was employed to identify the surface stoichiometry and elemental oxidation states in Mn doped ZnO nanocrystalline powders. The morphological features of nanocrystalline powders, along with the quantitative analysis of elements, were investigated using a JEOL JSM 6700 field emission scanning electron microscope (FESEM) coupled with Oxford instrument's energy dispersive x-ray (EDX) system. Furthermore, the magnetic characterization was performed by a Lakeshore 7404 vibrating sample magnetometer (VSM) at room temperature to study the ferromagnetic ordering in nanocrystalline powders.

III. RESULTS AND DISCUSSION

A. Structural analysis

Figure 1 shows the x-ray diffraction profiles of $Zn_{1-x}Mn_xO$ nanocrystalline powders for different concentrations of Mn (x = 0.02, 0.05, and 0.1). The XRD profiles have been indexed and found to be hexagonal wurtzite in structure with ten prominent peaks indicating a non-preferential orientation (polycrystalline) that is matched well with space group $P6_3mc$ (No. 186) (ICSD # 82028) of wurtzite ZnO. No traces of manganese oxides and/or any binary zinc-manganese phases are observed in any of the samples indicating the successful incorporation of Mn at the lattice sites of Zn in host ZnO matrix.

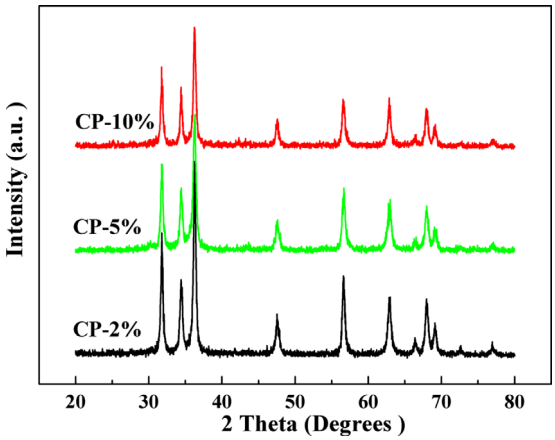

FIG. 1. (Color online) XRD diffraction profiles of ZnO:Mn nanocrystalline powders for different Mn concentrations.

Any impurity phase with concentration below the detection limit of XRD cannot contribute to RTFM in the samples, as none of these possible phases (e.g., Mn_3O_4, $ZnMn_2O_4$, etc.) is ferromagnetic at room temperature.[20,21] The reduction in diffraction peak intensity and increase in full width at half maximum (FWHM) with increasing Mn content suggest the nanocrystalline nature of the samples. The average crystallite size, determined from the broadening (FWHM) of diffraction peaks using Scherer formula, are found to be 10.4, 10.3, and 9.5 nm for CP-2%, CP-5%, and CP-10% samples, respectively. In addition, the shift in diffraction peak (refer Table I) with the increase in Mn content suggests the incorporation of tetrahedral Mn^{2+} ions at the substitutional sites of Zn^{2+} ions.[22] The peak shift towards lower angles is an important evidence of replacement of Zn^{2+} with Mn^{2+} ions.[23]

The incorporation of Mn^{2+} ions can also be verified by the change in lattice parameters and the cell volume as a function of Mn doping concentration. The lattice parameter "a" and the cell volume are found to increase with an increase in Mn content as shown in Figure 2 while there is a little change in the lattice parameter "c" (refer Table I). Both the lattice parameter "a" and the cell volume varied monotonically with the increase in Mn content and followed

TABLE I. FWHM and lattice parameter c of ZnO:Mn nanocrystalline powders.

Sample name	Centre of the peak	d-spacing (Å)	FWHM	Lattice parameter c(Å)	Bond length(Å)
CP-2%	36.272	2.4746	0.014031	5.203	1.9767
CP-5%	36.265	2.4751	0.014136	5.204	1.9769
CP-10%	36.261	2.4754	0.015436	5.203	1.9772

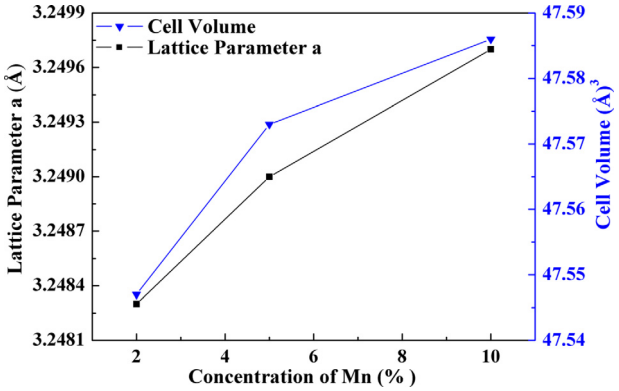

FIG. 2. (Color online) Variation of lattice parameter "a" and cell volume with Mn doping concentration.

Vegard's law.[3] The observed cell expansion indicates that the tetrahedral Zn^{2+} ions (0.74 Å) are replaced by larger sized (0.83 Å) tetrahedral Mn^{2+}ions.[24] Furthermore, the increase in interlayer distance (d-spacing) with the increase in Mn content also justifies the incorporation of tetrahedral Mn^{2+} at the lattice sites of Zn^{2+} (refer Table I). A consistent increase in bond length (refer Table I) is also an evidence of tetrahedral Mn^{2+} incorporation at Zn^{2+} lattice sites.

B. Optical analysis

Figure 3 shows the room temperature PL spectra of the nanocrystalline powders with different Mn contents. All PL spectra have similar features with two luminescence bands; the NBE and DLE bands. The UV emission, centered at ~380 nm, is attributed to the NBE free excitation transitions which can take place even at room temperature for ZnO. The intensity of NBE strongly depends on the Mn content.[25] In our case, the intensity of NBE decreases with the increase in Mn content that might be attributed to some non-radiative recombination processes.

The DLE band is attributed to defect states within the band gap of ZnO.[26] The DLE spectra for CP-2%, centered at ~600 nm, exhibits the signatures of yellow emission that is attributed to the presence of oxygen interstitials (O_i)[27] in Mn doped ZnO nanocrystalline powders while no DLE spectra

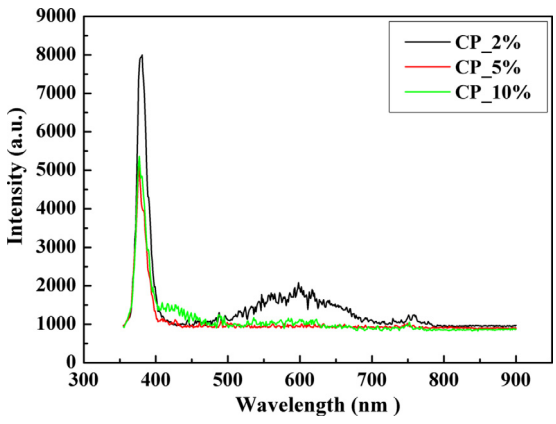

FIG. 3. (Color online) Room temperature photoluminescence spectra of Mn doped ZnO nanocrystalline powders.

was observed for CP-5%. For CP-10%, the DLE spectra was deconvoluted with three peaks, centered at ~408, 489, and 580 nm, respectively, using Gaussian function (not shown here). The deconvoluted peak at 408 nm is attributed to the transition from energy levels of interstitial zinc (Zn_i) to the valence band while the peak at 489 nm is related to the transition from energy level of singly ionized interstitial zinc (Zn_i) to local zinc vacancy (V_{Zn}) level. The peak at 580 nm exhibits the yellow emission that is attributed to the presence of oxygen interstitial (O_i) in nanocrystalline powders. Increased carrier concentration of Zn_i (estimated from the relative area under curve of the deconvoluted peak) is responsible for the change in ferromagnetic phase to paramagnetic in CP-10% (discussed later under the Sec. III E for magnetic properties) that is consistent with the Ruderman-Kittel-Kasuya-Yosida (RKKY) exchange model.[28]

C. Compositional analysis

The typical XPS Zn $2p_{3/2}$ core level spectrum of CP-5% is shown in Figure 4(a), with the binding energies being calibrated by adventitious C 1 s peak centered at ~284.6 eV. All the samples exhibit similar Zn $2p_{3/2}$ core level spectrum. The stoichiometery of nanocrystalline powders calculated from the relative area under the zinc and oxygen peaks, after a Shirley background subtraction by non linear least square fitting using mixed Gauss-Lorentz function, is found to be oxygen rich with $Zn/O < 1$ for all nanocrystalline powders.

The asymmetric Zn $2p_{3/2}$ peak of zinc in the elemental as well as oxide form usually consists of two sub-peaks (after deconvolution) centered at ~1022.4 and ~1021.5, respectively.[29] In our case, the two sub-peaks in deconvoluted core level peak of Zn $2p_{3/2}$ are located at ~1020.4 eV and ~1021.7 eV, as shown in Figure 4(a). The lower energy peak, in the deconvoluted spectrum of Zn $2p_{3/2}$, at ~1020.4 eV is attributed to the O^{2-} ions in the wurtzite structure of hexagonal Zn^{2+} ion array i.e. oxide form of Zn in nanocrystalline ZnO (Ref. 30) while the peak centered at ~1021.7 eV is attributed to metallic zinc. The shift in binding energy towards the lower value is due to the partial substitution of lattice Zn by Mn^{2+} ions in ZnO and Zn-Mn bonding structure.[31] Since the electro negativity of Mn ($\chi = 1.55$) is smaller than that of O ($\chi_o = 3.44$),[32] Zn atoms bonded to Mn atoms will contribute to the shift in the binding energy of Zn $2p_{3/2}$. Furthermore, the reduced crystallite size which broadens the peak also contributes to the shift in the binding energy towards the lower energy side.[30]

Figure 4(b) shows the typical Mn $2p_{3/2}$ core level XPS spectrum of CP-10% sample. All the samples exhibit the presence of manganese in its two oxidation states. The Mn $2p_{3/2}$ peak, centered at ~641.2 eV, was deconvoluted into two components centered at ~640.9 and ~643.0 eV using Gausssian peak fitting. The first peak centered at ~640.9 eV confirmed the presence of Mn^{2+} in the host lattice of ZnO while the second peak centered at ~643.0 eV is attributed to the presence of Mn^{4+} oxidation state.[33] Furthermore, the contribution of the peak at ~640.9 eV increased from 35% for CP-2% to 88% for CP-10%, respectively (calculated from the relative area under curve of the peak fitted with

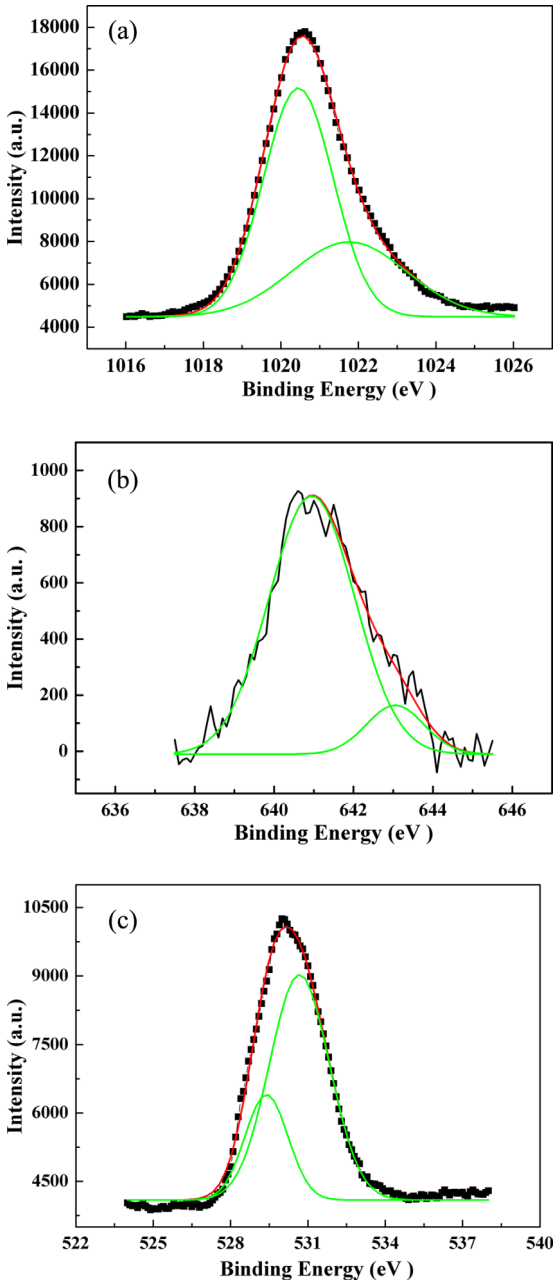

FIG. 4. (Color online) XPS core level spectra of (a) Zn $2p_{3/2}$ of CP-5% sample, (b) Mn $2p_{3/2}$ of CP-10% sample, and (c) O 1 s of CP-10% sample deconvoluted with two peaks using Gaussian peak fitting.

Gaussian function) which in turn validates the enhanced concentration of Mn^{2+} in higher doped samples.

Figure 4(c) shows the asymmetric O 1s peak of CP-10% which is deconvoluted with two peaks centered at ~529.5 eV and 530.6 eV. Similar features were observed for all other samples with the exception of CP-2% in which an additional peak (531.7 eV) related to O_i was observed. The lower energy peak is attributed to the O^{2-} ions in the wurtzite structure of the hexagonal Zn^{2+} ion array. Therefore, the lower energy peak of oxygen spectrum can be attributed to Zn-O bonds.[34] The peak at ~530.6 eV is attributed to O^{2-} ions in oxygen deficient regions and is related to the presence of oxygen vacancies (V_o). The contribution of Zn-O bonds, estimated from the relative area under the peak at 529.5 eV, was observed to be 31%, 42%, and 25% for CP-2%, CP-5%, and CP-10%, respectively. The maximum value (42%) in CP-5% reveals an enhanced concentration of oxygen in Zn-O bonding that will minimize the contribution from V_o towards the ferromagnetic signal for this sample.

D. Morphological analysis

The FESEM micrographs, shown in Figure 5, reveal a clear distinction between the grain boundaries of different nano-sized particulates with their well-defined dimensions along the surface of the nanocrystalline powders. The average particle size was estimated to be $\sim 36.3 \pm 2.4$ nm, $\sim 33.2 \pm 2.0$ nm, and $\sim 31.8 \pm 1.2$ nm for CP-2%, CP-5%, and CP-10%, respectively, using image processing (image J®) software. The reduction in average particle size from about 36 nm to about 32 nm, with the increase in Mn content from 2 at. % to 10 at. %, is attributed to the incorporation of Mn ions as there is an inverse relation between the particle size and the ionic radius of metallic ions.[35] Furthermore, the increase in Mn concentration resulted in uniform distribution of narrow-sized particles with well-defined grain boundaries leading to improved surface features of the nanocrystalline powders. A large percentage of all the atoms in a nanoparticle (with decreasing particle size) are surface atoms, which implies that interface and surface effects turn out to be more important.[36] Owing to large surface atoms/bulk atoms ratio, the surface spins make an important contribution to the magnetization. Surface effects can lead to a reduction in magnetization of smaller particles which might be associated with different mechanisms, such as the existence of a magnetically dead layer on the particle's surface, the existence of canted spins, or the existence of a spin glass like behavior of the surface spins.[36] The decreasing size of nanoparticles with increasing Mn doping concentration, as estimated through FESEM images, indicates the increasing number of surface atoms and thereby suggests the possible reduction in ferromagnetism. However, as the reduction in nanoparticle size with Mn concentration is only marginal, therefore, its effect on ferromagnetic property will not be too significant if other mechanisms, as discussed in Sec. III E, have more profound effect.

The typical EDX spectrum of CP-10% with elemental compositional analysis, shown in Figure 5(d), exhibits the presence of all key elements i.e. Zn, O, and Mn. The quantitative EDX measurement shows 5.69 and 2.97 at. % of Mn for CP-10% and CP-5% samples, respectively, which is less in comparison to the doping concentration used for these samples. No signature of Mn has been found for CP-2% as EDX is insensitive for the detection of elements below 2 at. %. The quantitative analysis of all the samples also reveals the dominance of oxygen over zinc showing oxygen rich stoichiometery of nanocrystalline powders, which is also validated by XPS results.

E. VSM analysis

The field dependence of magnetization (M), at room temperature, for nanocrystalline powders is studied using VSM in the applied magnetic field range of 0-3000 G. The

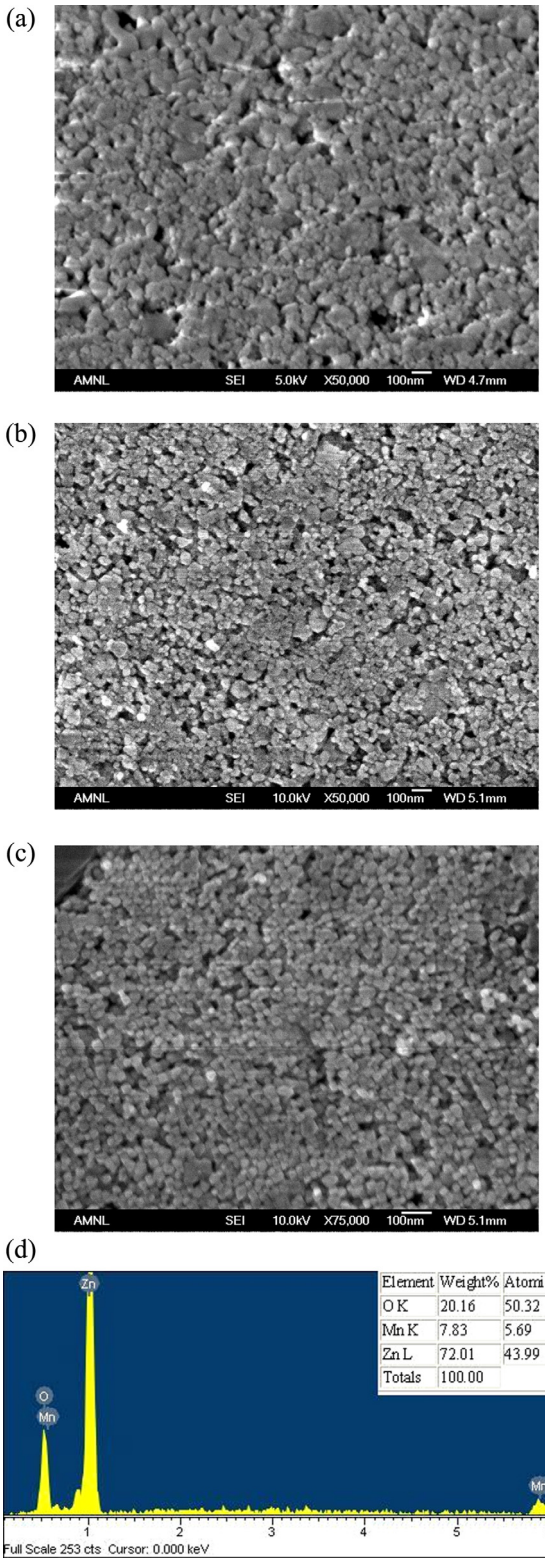

FIG. 5. (Color online) FESEM micrographs of (a) CP-2%, (b) CP-5%, (c) CP-10%, and (d) EDX spectra with elemental concentration of CP-10% nanocrystalline powder.

M-H curves of CP-2% and CP-5% exhibit RTFM while for CP-10%, the competing mechanism of paramagnetic phase is dominant (refer Figures 6–8). The variation in saturation magnetization (M_s), remanant magnetization (M_r), and coercivity along with magnetic moment (μ_B) for different Mn doped samples is presented in Table II.

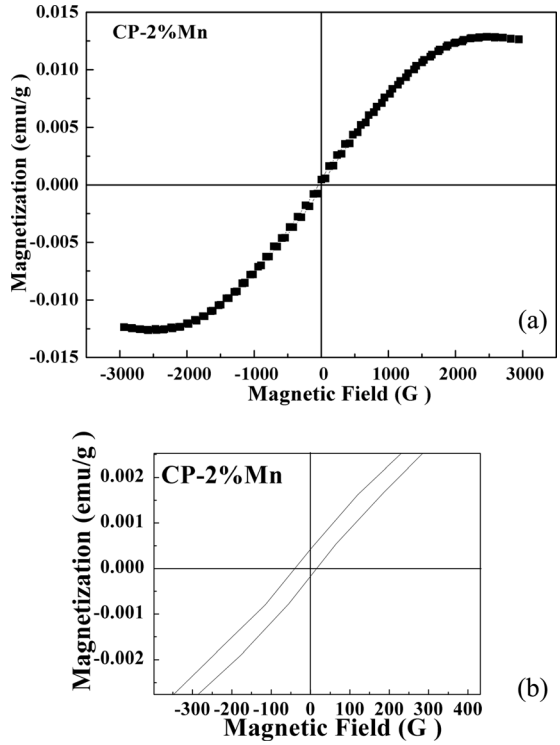

FIG. 6. Field dependent M-H curves of CP-2% nanocrystalline powder exhibiting ferromagnetic ordering with (b) showing clear retentivity.

The maximum value of magnetic moment per Mn atom was achieved for CP-5% sample but it is much smaller than the reported value of Mn^{2+} state ($5\,\mu_B$/Mn atom).[17] The reduced value of magnetic moment might be attributed to the anti-ferromagnetic coupling between the neighboring Mn atoms that reduce the ferromagnetic signal. Furthermore, the presence of isolated Mn atoms, which are paramagnetic in nature,[17] can also contribute to suppress the ferromagnetic signal.

Figures 6 and 7 reveal the dependence of magnetization on the applied magnetic field for CP-2% and CP-5% nanocrystalline powders exhibiting RTFM. According to the bound magnetic polaron model (BMP), bound electrons in defects, like oxygen vacancies (V_o), can couple with Mn ions and cause ferromagnetic regions to overlap giving rise to long range ferromagnetic ordering in the samples. In accordance with BMP model, the magnetization of the system originates from the regions of correlated and isolated spins. The magnetization that arises from correlated spins is ferromagnetic (M_{FM}), whereas the magnetization due to uncorrelated spins is paramagnetic (M_P).[18] So, based on BMP model, the RTFM might be attributed to V_o. According to this theory of defect mediated RTFM, the saturation magnetization and ferromagnetic signal should decrease for CP-5% sample as there is no signature of V_o in corresponding DLE spectra (Figure 3). The increased saturation magnetization (Figure 7) and minimum defects concentration in CP-5% sample rules out the contribution of V_o towards the ferromagnetic signal.

The RTFM in ZnO:Mn nanocrystalline powders can also be explained on the basis of RKKY interaction which explains the magnetic phases based on the concentration of

TABLE II. Different magnetic parameters of nanocrystalline powders.

Sample name	M_s (emu/g)	M_r (emu/g)	Coerisivity (G)	N_{Mn}/g	μ_B/Mn atom	Susceptibility $\chi = M/H$ (emu/g.G)
CP-2%	0.0127	297.91×10^{-6}	27.772	0.79×10^{20}	0.21	6.12×10^{-6}
CP-5%	0.0350	524.03×10^{-6}	31.224	2.00×10^{20}	0.23	10.71×10^{-6}
CP-10%	0.0175	149.59×10^{-6}	17.537	4.01×10^{20}	0.06	5.36×10^{-6}

free carriers apart from the concentration of magnetic ions. ZnO is a native n-type material due to V_o and Zn_i. However, to achieve ferromagnetism in case of Mn doped ZnO, the electron concentration must be low.[4] Dietl's mean field calculations[4] predict that the RTFM is possible in Mn-doped ZnO that is heavily doped with holes, while the carrier mediated ferromagnetism in n-type material should be limited to lower temperatures.[37] Furthermore, the addition of electrons to the system will move the Fermi energy level up in the band gap, resulting a decrease in hole density and a reduction in magnetization. In our case, oxygen rich stoichiometery with increased Zn-O bonding in Mn doped ZnO nanoparticles favors the indirect Mn-O-Mn ferromagnetic exchange coupling. Furthermore, the enhanced Zn-O bonding in CP-2% and CP-5% (refer XPS analysis) in turn reduces the V_o (donors) and leads to strong hybridization (p-d exchange coupling) of Mn in ZnO host matrix which is responsible for RTFM. It may, however, be noted that for CP-2% sample, the presence of DLE (~600 nm) in PL spectra and XPS peak at ~531.7 eV indicates the presence of O_i (acceptors) which according to Dietl's prediction[4] might also contribute towards the ferromagnetic ordering for this sample as holes are required to mediate RTFM in Mn doped ZnO. However, the VSM data showed that the ferromagnetism in CP-5% samples (with highest Zn-O bonding concentration) is stronger than that of CP-2% indicating that the ferromagnetic contribution of Mn-O-Mn exchange coupling due to Zn-O bonding is much more significant as compared to defected mediated ferromagnetism.

Of course, there is still a possibility of occurrence of an anti-ferromagnetic ordering of spins, but its probability is very small[38] specifically for CP-2% and CP-5% samples due to the lower concentration of Mn ions for these samples.

It is well known that Mn ions belonging to anti-ferromagnetic clusters do not contribute to the increase in magnetic signal rather they reduce the net magnetization.[22] Among all oxides of Mn, only MnO is anti-ferromagnetic with a Neel temperature of 96 K and Mn_3O_4 is ferromagnetic with a curie temperature of 43 K. But in our case, the reduction in magnetization due to nano-clustering or secondary phase formation is ruled out as any impurity phase regarding Mn clustering was not observed in our XRD spectra. Therefore, the RTFM in nanocrystalline powder is from the ferromagnetic interaction between adjacent Mn ions that substitute the Zn ions rather than nanoclustering of Mn oxides or contribution from V_o.

It is reported that Zn_i produced at lower temperature annealing can also cause RTFM,[32] but in our case, this reasoning is also ruled out as CP-10% does not show any RTFM (as seen in Figure 8) though its DLE spectra show the presence of Zn_i (refer PL analysis). In CP-10%, the average distance between the adjacent Mn atoms decreases due to the increased concentration of Mn (10 at. %), which will favor super exchange Mn-Mn interaction. The exchange coupling between Mn-Mn nearest neighbors in ZnO is believed to be anti-ferromagnetic[39] due to overlapping of Mn d-states with the valence band. As the anti-ferromagnetic energy is lower

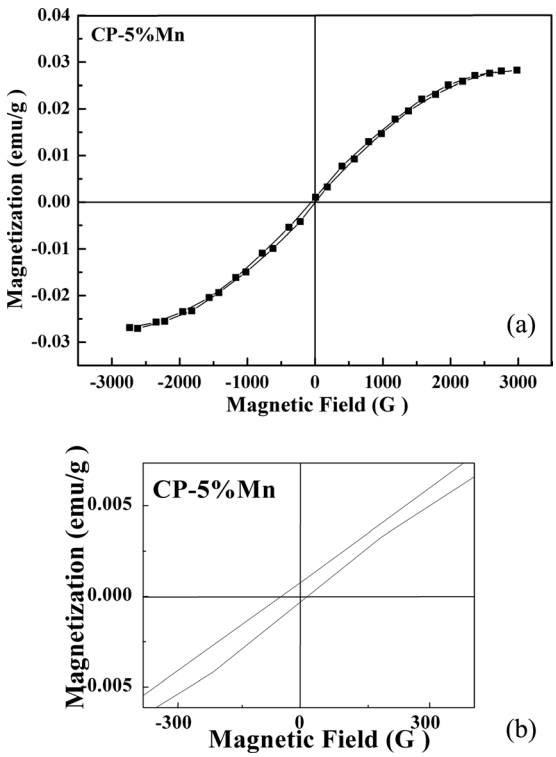

FIG. 7. Field dependent M-H curves of CP-5% nanocrystalline powder exhibiting ferromagnetic ordering with (b) showing clear retentivity.

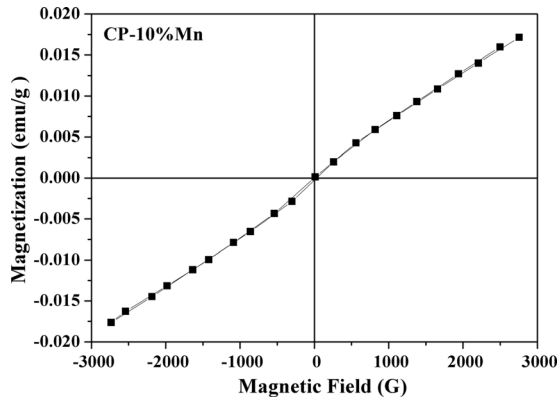

FIG. 8. Field dependent M-H curve of CP-10% nanocrystalline powder exhibiting dominant paramagnetic phase.

than the ferromagnetic one due the reduced distance between the adjacent Mn ions, most of the Mn atoms should be anti-ferromagnetically coupled at the relatively higher Mn concentrations (10 at. % Mn). Small signature of ferromagnetic signal in CP-10% (Figure 8) might be attributed to the V_{Zn} that is likely to occur in Mn doped ZnO matrix. For Mn doped ZnO with V_{Zn}, the acceptor band shows a large spin-split with spin up defect state of V_{Zn}.[40] According to the BMP model, the charge transfer between hybridized Mn 3 d state and V_{Zn} induced defect state favors the RTFM.[40] Direct exchange coupling of Mn ions (Mn-Mn) is anti-ferromagnetic due to overlapping of Mn d-states while the indirect coupling of Mn ions (Mn-O-Mn) is ferromagnetic. Direct anti-ferromagnetic coupling competitions, between adjacent d-shells of Mn ions, suppress the ferromagnetic signal exhibited due to indirect exchange coupling. So, there are likely competing mechanisms between regions of Mn-defect pair ferromagnetism, Mn-Mn nearest-neighbor anti-ferromagnetism, and isolated manganese atoms that act paramagnetically.

The increased carrier concentration of native defects (like Zn_i) for CP-10% is also responsible for suppressing the ferromagnetic phase that might transform it to the paramagnetic phase. This is consistent with the proposed model for Mn-doped ZnO,[4] where ferromagnetic ordering is not favored by increase in electron concentration.

IV. CONCLUSION

The oxygen rich nanocrystalline ZnO:Mn powder was prepared by simple wet chemical method using zinc acetate dihydrate and manganese acetate tetrahydrate as precursors for Zn and Mn species instead of normally used solid-state reaction method. The XRD spectra showed cell expansion in higher doped nanocrystalline ZnO powders with a consistent increase in interlayer spacing, suggesting the incorporation of larger sized tetrahedral Mn^{2+} ions at the lattice sites of Zn^{2+} ions. The detailed XPS analysis of Zn 2 p and Mn 2 p core level spectra reveals the maximum incorporation of Mn at the lattice sites of Zn for CP-5% sample resulting in enhanced saturation magnetization (0.04 emu/g) with RTFM. The absence of DLE spectra for CP-5% indicated that the RTFM for this sample was not due to structural defects (oxygen vacancies and zinc interstitials) rather induced intrinsically by the incorporation of Mn^{2+} ions, a prerequisite for spintronic devices. Furthermore, the FESEM micrograph revealed the existence of well-defined nano-sized (32-36 nm) particles in Mn doped nanocrystalline powders with improved surface features consistent with the XRD results indicating the reduction in average crystallite size of the particles with Mn incorporation.

ACKNOWLEDGMENTS

This project was supported by the AcRF Grant (RI 7/08 RSR) provided by NIE, Nanyang Technological University Singapore. One of the authors, Usman Ilyas, is grateful to the University of Engineering & Technology Lahore for providing fully funded research scholarship under Faculty Development Program (FDP) of Higher Education Commission (HEC) of Pakistan.

[1]S. A. Wolf, D. D. Awschalom, R. A. Buhrman, J. M. Daughton, S. V. Molnar, M. L. Roukes, A. Y. Ctchelkanova, and D. M. Treger, Science **294**, 1488 (2001).
[2]H. Ohno, Science **281**, 951 (1998).
[3]J. K. Furdyna, J. Appl. Phys. **64**, R29 (1988).
[4]T. Dietl, H. Ohno, F. Matsukura, J. Cibert, and D. Ferrand, Science **287**, 1019 (2000).
[5]L. L. Ren and Y. J. Won, Rare Met. **25**, 51 (2006).
[6]D. S. Reddy, S. K. Sharma, Y. D. Reedy, K. R. Gunasekhar, and P. S. Reddy, J. Optoelectron. Adv. Mater. **10**, 2607 (2008).
[7]A. M. A. Hakeem, J. Magn. Magn. Mater. **322**, 709 (2010).
[8]P. Sharma, A. Gupta, F. J. Owens, A. Inoue, and K. V. Rao, J. Magn. Magn. Mater. **282**, 115 (2004).
[9]P. Sharma, A. Gupta, K. V. Rao, F. J. Owens, R. Sharma, R. Ahuja, J. M. O. Guillen, B. Johansson, and G. A. Gehring, Nature Mater. **2**, 673 (2003).
[10]S. Karamat, S. Mahmood, J. J. Lin, Z. Y. Pan, P. Lee, T. L. Tan, S. V. Springham, R. V. Ramanujan, and R. S. Rawat, Appl. Surf. Sci. **254**, 7285 (2008).
[11]Y. Q. Chang, D. B. Wang, X. H. Luo, X. Y. Xu, X. H. Chen, L. Li, C. P. Chen, R. M. Wang, J. Xu, and D. P. Yu, Appl. Phys. Lett. **83**, 4020 (2002).
[12]D. B. Norton, S. J. Pwarton, A. F. Hebard, N. Theodoropoulou, L. A. Boatner, and R. G. Wilson, Appl. Phys. Lett. **82**, 239 (2003).
[13]A. K. Pradhan, K. Zhang, S. Mohantry, J. B. Dadson, D. Hunter, J. Zhang, D. J. Sellmyer, U. N. Roy, Y. Cui, A. Burger, S. Mathews, B. Joseph, B. R. Sekhar, and B. K. Roul, Appl. Phys. Lett. 86, 152511 (2005).
[14]S. S. Kim, J. H. Moon, B. T. Lee, O. S. Song, and J. H. Je, J. Appl. Phys. **95**, 454 (2004).
[15]T. Fukumura, Z. Jin, M. Kawasaki, T. Shono, T. Hasegawa, S. Koshihara, and H. Koinuma, Appl. Phys. Lett. **78**, 958 (2001).
[16]A. Tiwari, C. Jin, A. Kvit, D. Kumar, J. F. Muth, and J. Narayan, Solid State Commun. **121**, 371 (2002).
[17]S. Chattopadhyay, S. K. Neogi, A. Sarkar, M. D. Mukadam, and S. M. Yusuf, J. Magn. Magn. Mater. **323**, 363 (2011).
[18]M. El-Hilo and A. A. Dakhel, J. Magn. Magn. Mater. **323**, 2202 (2011).
[19]J. H. Li, D. Z. Shen, J. Y. Zhang, D. X. Zhao, B. S. Li, Y. M. Lu, Y. C. Liu, and X. W. Fan, J. Magn. Magn. Mater. **302**, 118 (2006).
[20]W. Yan, Z. Sun, Q. Liu, Z. Li, Z. Pan, D. Wang, Y. Zhou, and X. Zhang, Appl. Phys. Lett. **91**, 062113 (2007).
[21]C. Liu, F. Yun, and H. Morkoc, J. Mater. Sci.: Mater. Electron. **16**, 555 (2005).
[22]G. Lawes, A. S. Risbud, A. P. Ramirez, and R. Seshadri, Phys. Rev. B **71**, 45201 (2005).
[23]K. Ueda, H. Tabata, and T. Kawai, Appl. Phys. Lett. **79**, 988 (2001).
[24]J. Anghel, A. Thurber, D. A. Tenne, C. B. Hanna, and A. Punnoose, J. Appl. Phys. **107**, 09E314 (2010).
[25]U. Ilyas, R. S. Rawat, G. Roshan, T. L. Tan, P. Lee, S. V. Springham, S. Zhang, F. Li, R. Chen, and H. D. Sun, Appl. Surf. Sci. **258**, 890 (2011).
[26]U. Ilyas, R. S. Rawat, T. L. Tan, P. Lee, R. Chen, H. D. Sun, F. Li, and S. Zhang, J. Appl. Phys. **110**, 093522 (2011).
[27]L. Schmidt-Mende and L. Macmanus-Driscoll, J. Mater. Today **10**, 40 (2007).
[28]D. P. Joseph, G. S. Kumar, and C. Venkaterwaran, Mater. Lett. **59**, 2720 (2005).
[29]K. G. Saw, K. Ibrahim, Y. T. Lim, and M. K. Chai, Thin Solid Films **515**, 2879(2007).
[30]Y. Y. Taya, S. Lib, C. Q. Sun, and P. Chen, Appl. Phys. Lett. **88**, 173118 (2006).
[31]C. J. Cong, L. Liao, J. C. Li, L. X. Fan, and K. L. Zhang, Nanotechnology **16**, 981 (2005).
[32]W. Xiao, Q. Chen, Y. Wu, T. Wu, and L. Dai, Mater. Chem. Phys. **123**, 1 (2010).
[33]S. R. S. Kumar, M. N. Hedhili, H. N. Alshareef, and S. K. Asiviswanathan, Appl. Phys. Lett. **97**, 111909 (2010).
[34]P. T. Hsieh, Y. C. Chen, K. S. Kao, and C. M. Wang, Appl. Phys. A: Mater. Sci. Process. **90**, 317 (2008).
[35]A. M. Samy, E. Gomaa, and N. Mostafa, Open Ceram. Sci. J. **1**, 1 (2010).
[36]A. H. Lu, E. L. Salabas, and F. Schuth, Angew. Chem. Int. Ed. **46**, 1222 (2007).
[37]R. P. Davies, C. R. Abernathy, S. J. Pearton, D. P. Norton, M. P. Ivill, and F. Ren, Chem. Eng. Commun. **196**, 1030 (2009).
[38]J. M. D. Coey, M. Venkateshan, and C. B. Fitzgerald, Nature Mater. **4**, 173 (2005).
[39]D. Iusan, B. Sanyal, and O. Eriksson, Phys. Rev. B **74**, 235208 (2006).
[40]Y. Jiang, W. Yan, Z. Sun, Q. Liu, Z. Pan, T. Yao, Y. Li, Z. Qi, G. Zhang, P. Xu, Z. Wu, and S. Wei, J. Phys.: Conf. Ser. **190**, 012100 (2009).